International Council for the
Exploration of the Sea ICES CM 2002 / P: 04
ICES / CIEM

Typology of surface currents in Biscay as produced by a circulation model, 1985-2000.

by

Pierre Petitgas, and Pascal Lazure

In Biscay, residual surface (10 m) currents on the shelf are predominantly due to salinity gradients coming from the river outflows and wind regimes. The model developed at IFREMER for the French shelf of Biscay is forced by real measurements of river outflow and wind. The model outputs for the period 1985-2000 allow for the typology of currents. Flow fields are no trivial objects: at each point of the model grid and each moment of the model output the data is made of a vector with particular direction and intensity; this vector is correlated in time with the vector at the same point occurring some time before and after; it is also correlated in space with vectors occurring in the vicinity of the point considered. At each point we considered the annual hodograph of the current, i.e. the annual vectorial sum of the current at the point. We constructed a particular distance between hodographs which represented a compromise between differences in orientation of the current as well as differences in its intensity. We performed a hierarchical classification of hodographs using this distance. Types of hodographs were then mapped geographically and differences between years quantified. A general flow towards the south was evidenced except in areas under the influence of the river outflows. Years could be classified using the flow field typology. The analysis could serve as a basis to incorporate indicators of the flow field in studies on recruitment variability to quantify the impact of larval drift.

P. Petitgas: IFREMER, Laboratory for Fisheries Ecology, BP 21105, rue de l'ile d'Yeu, 44311 cdx 3, Nantes, France [tel: +33 240 374000, fax: +33 240 374075, e-mail: pierre.petitgas@ifremer.fr]. P. Lazure: IFREMER, DEL/AO, BP 70, Pointe du Diable, 29280 Plouzané, France [tel: +33 298 224341, fax: +33 298 224555, e-mail: pascal.lazure@ifremer.fr]

Introduction

Flow fields are rarely surveyed on grids of fixed stations at large scale. Such design would require the deployment of a great number of fixed instrumented buoys during long periods of time which would interfere with navigation and fishing. Also, in European waters where tidal currents are the most important component of the instantaneous current, the signal measured at sea would need to be filtered to estimate the residual current and this would require long periods of measurement. Therefore flow fields delivered as series of maps in space and time can only be provided by 3D hydrodynamic models.

The 3D hydrodynamic model developed at IFREMER over the French continental shelf in the bay of Biscay simulates realistically temperature, salinity, density and current flow fields (Lazure and Jégou, 1998). The model allows for the integration of the non linear interactions between the many factors generating advection and mixing. The most important factors in Biscay are the varying wind regimes, the varying salinity gradients due to the outflow of two big rivers, Loire and Gironde, and tidal currents. The model has been validated for temperature and salinity using maps of temperature of both satellites and field surveys; maps of salinity of surveys; as well as using time series at particular stations for both temperature and salinity.

The biological interest in flow fields is their potential importance in determining migration routes (for accessing spawning grounds and nursery grounds) and larval drifts as well as in explaining their variability. Flow fields also represent a general dynamical condition on the fish habitats and are therefore important to characterise. The object of the present paper is to make a typology of the flow fields over the French shelf of Biscay. For that purpose we used the residual currents estimated by the hydrodynamic model for the area and the period 1985-2000. At each point, we considered the vectorial sum of the current over the year which is an hodograph of the current at the point. Hodographs were a simple way to summarise the evolution of the current at each point. Years and locations were compared and classified based on differences between hodographs. Therefore we considered a particular distance between hodographs allowing for the characterisation of the differences both in direction and intensity of the currents. Questions to be answered were: (i) what are the different separable types of hodographs of currents; (ii) what is the probability to encounter a given hodograph type at a given location and (iii) can the years be classified based on the typology of hodographs of currents. The study was undertaken on the surface currents (u,v) at 10 m depth.

Material and Method

3D hydrodynamic model. Description of the model in Lazure and Jégou (1998), Allain et al. (2001). The model was run for the period 1985-2000, using realistic forcings for wind, tides and river outflow. Outputs were delivered on the model 3D grid as 2 day averages. The area considered was the French shelf in Biscay, from coast to 200 m depth and from 48°N (Pointe de Pen marc'h) to 44°N (Gouf de Cap Breton).

Hodographs of surface currents. For the present study we considered only 1 point out of 6 on the, making 94 points on a regular grid of approximately 30 km x 30 km. We considered the horizontal current components u and v at 10 m depth. One coastal point near the Gironde estuary had a bottom depth of 7 m and was omitted from the study which was thus performed on 93 points (Fig. 1). The components u and v were averaged over fixed periods of approximately 5 days providing 6 values per month resulting in 72 vectors per year at each of the 93 points. The 5 day period was found a relevant period in a previous study (Allain et al. 2001). In each year, at each point, the 72 components u and v were respectively summed to produced the cumulative current (hodograph) which summarised the yearly evolution of the current at each point.

Distances between hodographs. Any classification is based on a distance between the objects to be classified. An hodograph being a cumulative vectorial sum, different distances are possible based on

the vector intensity at the nodes of the hodograph or on its orientation. Dazy and Lebarzic (1996) compared different distances in analysing the classification of trajectories of observations in evolutionary multi-table analysis. The hodograph *i* is defined as a suite of dates *(t=1, …, T)* at which we have a position $x_t(i) = (u_t(i) , v_t(i))$.

The distance position between hodographs *i* and *j* is based on the Euclidean distances at each of their nodes *t*. It is defined by:

$$d_p{}^2(i,j) = \sum_{t=1}^{T} [x_t(i) - x_t(j)]^2 = \sum_{t=1}^{T} P_{i,j}(t)$$

The distance evolution between hodographs *i* and *j* is based on the difference in orientation between two successive nodes *t* and *t-1*:

$$d_e{}^2(i,j) = \sum_{t=2}^{T} [(x_t(i) - x_{t-1}(i)) - (x_t(j) - x_{t-1}(j))]^2 = \sum_{t=2}^{T} E_{i,j}(t)$$

Both distances satisfy the mathematical definition of a distance. The distance position will keep in memory the large difference in position that may have occurred at one node of the hodograph. The distance evolution has no such effect. It will be small for hodographs that may depart in space but have similar orientations. Inertia I_p and I_e can be defined for each of the distances position and evolution as the summed differences between individual hodographs and the average hodograph indexed by *m*:

$$I_p = \sum_{i=1}^{N} \sum_{t=1}^{T} P_{i,m}(t) = \sum_{t=1}^{T} I_p(t) \; ; \; I_e = \sum_{i=1}^{N} \sum_{t=2}^{T} E_{i,m}(t) = \sum_{t=2}^{T} I_e(t)$$

Dazy and Lebarzic (1996) defined a distance compromise between position and evolution. At each node of the hodograph, one switches either to the position or the evolution term depending on a criteria:

$$d_{cs}{}^2(i,j) = P_{i,j}(1) + \sum_{t=2}^{T} \alpha_t P_{i,j}(t) + (1-\alpha_t) E_{i,j}(t)$$

The coefficient α_t is either equal to *0* or *1* depending which term is retained at node *t*. Which criteria to use to define the suite α_t *(t=1,…T)* ? We chose the following criteria which increased the causes of variation between hodographs:

If $I_p(t)/I_p \geq I_e(t)/I_e$ then $\alpha_t=1$; otherwise $\alpha_t=0$.

The compromise distance with this criteria was used by Petitgas (2002) when classifying hodographs of wind as well as individual growth curves and was found to generate classes with larger inter-group inertia than other distances.

Classification of hodographs and maps of hodograph types. The distance compromise was computed between all hodographs resulting in a matrix of 1488 by 1488 (16 years and 93 points). The hodographs were then classified using hierarchical clustering with the compact method (Lebart et al. 1995). This method results in more spherical groups than other methods. The hierarchical tree allowed for choosing the number of groups of hodographs. In each group, the average hodograph was estimated and groups were mapped. Probability maps of hodograph group occurrence were estimated by estimating the number of times (years) the same group of hodograph occurred at each station. Also, yearly maps were compared based on the difference in the spatial frequency of the different groups of hodographs.

Results

Inertia position and evolution and configuration of the distance compromise. Pooling all years and all points, the average hodograph was computed as well as the inertia I_p and I_e corresponding to the distances position and evolution (Fig. 2). The distance evolution shows greater variability in winter

and autumn and less in summer, meaning that the hodographs tend to have similar orientation in summer. The distance position accumulates with time the memory of the variation between hodographs. Differences between hodographs are generated by differences in their orientation in the first semester, then the distance position takes in charge the differences (Fig. 3). Based on that figure and the previously defined rule for determining the coefficients α_t *(t=1,…T)* of the distance compromise, the suite of α_t was: $\alpha_t = 0$ for $t<41$; $\alpha_t = 1$ otherwise.

Average hodograph and inertia at each point. At each point, we had 16 annual hodographs (1985-2000). The average hodograph at each station was estimated and the inertia around it corresponding to the distance compromise (Fig. 4). Although the average can be misleading because hodographs going in different directions may result in a confusing average, a spatial pattern is clearly visible. North of 47°N outside the 100 m isobath, currents go to the SE with low variability between years. Inshore of the 100 m depth and between 45°N and 48°N, a much greater variability is observed between years. In that area, the general pattern is a current going to the NW in the first months of the year then going to the SW in summer and returning to the NW in autumn. Occasionally at coastal stations, currents go to N or to the coast. Inside the 100 m depth along the coast of Les Landes (44°N – 45°N), the current goes to the S with a high inter-annual variability. Centred on the 100 m isobath at 45°N currents go to the N with a high inter-annual variability.

Classification of hodographs. The distance compromise was computed between all pairs of hodographs, irrespective of year and station (i.e., inter-annual and spatial variations were pooled). The hierarchical classification performed based on these distances provided a classification in 6 groups (Fig. 5 and 6). The intra-group inertia amounted to 21.5 percent of the total inertia making the classification in 6 groups a satisfactory summary (typology) of the major differences in the hodographs. Group 1 was made of the hodographs going to the N. Group 2 was made of the hodographs going to the SE. Group 6 was the same as Group 2 but with a higher intensity in the current. Group 3 was made of hodographs going to the SSE. Group 4 was made of hodographs going to the NNW in winter, NW in spring, then to the SW in summer and returning to the NNW in autumn. Group 5 was made of hodographs going to the NE in winter, then going to the E and returning to the NE in autumn. Groups 1, 2, 3, 4 represented the most frequent hodograph types and types 2, 4 and 3 represented 86% of all hodographs (Table 1).

Probability maps of hodograph group occurrence. At each station, we had 16 annual hodographs. These belonged either to the same hodograph type or to different ones, allowing for the mapping of the inter-annual probability of hodograph type occurrence (Fig. 7). No group occurred with an inter-annual probability less than 0.25. Most probable groups (prob. 0.75 – 1) were groups 2, 4 and 3 spatially distributed with a strong pattern: group 2 was outside the 100 m isobath north of 46°30N. North of 45°N and inside the 100 m isobath, group 4 dominated. South of 45°N (shelf of Les Landes) group 3 occurred at the coastal stations. Less probable groups (prob. 0.5 – 0.75) were centred on the 100 m isobath and were represented by groups 2 and 4 in north Biscay (north of 45°N) and group 1 near 45°N. The map of highest probability at each point provides a synthetic picture of the currents (Fig. 8). North of 45°N, Group 2 dominates outside the 100 m isobath; group 4 dominates the inner and centre shelf. South of 45°N, group 3 is coastal and group 1 occurs in the centre shelf near 45°N.

Classification of years. The spatial frequency of each hodograph type in each year (Table 1) was a measure of the spatial extension of the hodograph type (Table 1). Differences between years *i* and *j* in the frequency of each hodograph group, f_g, was estimated by the Euclidean distance between each line of Table 1 :

$$d^2(i,j) = \sum_{g=1}^{6} \left[f_g(i) - f_g(j) \right]^2$$

The distance served to classify the years (Fig. 8 and Table 2). 3 groups of years were retained. Group 1 was made of years: 1988, 1989, 1993, 1995, 1996, 1997; group 2 was made of the years: 1987, 1990, 1991, 1992, 1994, 1998, 1999, 2000; and group 3 was made of the years: 1985, 1986. Hodograph types 5 and 6 had no influence in the classification of years, meaning that hodograph types 1 to 4 were

the structuring types. Group 3 of years showed no hodograph type 3 and the currents during these years were dominated by hodograph type 2. Group 1 of years showed the more balanced representation of hodographs types 1 to 4. In group 2 of years, hodograph type 1 was little represented to the favour of hodograph type 2.

Conclusion – Discussion

The methodology used (annual hodographs of currents and a particular distance between hodographs accounting both for intensity and orientation of vectors) provided a synthetic summary of the major types of currents on the French shelf in Biscay. The study also enabled to classify years based on the maps of types of currents.

The types of currents could be interpreted considering the interaction between wind and salinity gradient. Hodograph of type 2 which dominated the outer shelf North of 45°N was thought to be generated mainly under the influence of W winds making the current go to the SE. Hodograph of type 4 which dominated the inner and central shelf was thought to be generated by river outflows in winter making the current go to the NW, by NW winds in summer making the current go SW and again by river outflows in autumn making the current come back to the NW. In the centre shelf north of 45°N, group 4 had varying occurrence between years meaning that the river outflows had varying influence between years in the centre shelf. Hodograph of type 1 near 45°N in the centre shelf was thought to be associated with gyres around low salinity lenses coming from the Gironde river outflow: the current would go to the N at these particular stations when it goes to the S and W at other stations in their vicinity. Hodograph of type 3 which was characteristic of the coastal stations off Les Landes (44-45°N) was thought to be associated with the coastal upwelling under the influence of the N winds in that area making the current to go SSE. It could be of interest to perform experiences with the hydrodynamic model using defined climatic regimes in order to interpret better the generation of the different hodograph current types.

The interest in the hydrodynamic model is that it computes the complex interaction between forcing climatic variables, here mainly wind and river outflow which vary seasonal and inter-annually. The study enabled to draw the contours of the areas that are under the influence of the wind regime or the river outflow with highest probability. The 100 m isobath resulted to be such limit north of 45°N. The study also enabled to characterise differences between years based on the variability in the maps of hodographs of currents. Years with no group 3 and years with no group 1 and large group 2 were thought to have corresponded with years with no upwelling and years with low river outflow influence offshore.

The analysis of the concordance between the classification of years based on the forcing climatic variables of the model and that based on the model results which estimate what occurs in the sea could be undertaken. But it seems as appropriate to perform experiments with the model for understanding the climatic situations generating a given pattern in the currents.

The circulation pattern provided in this study could be the basis for incorporating simple flow field parameters in the statistical analysis of inter-annual recruitment variability and thus quantify the impact of larval drift in the recruitment processes of different species in Biscay.

Acknowledgements

This study was a contribution to the IFREMER research program on Resource Variability, project FOREVAR affiliated to GLOBEC. It was supported by the French national research program for shelf ecology (PNEC) and the IFREMER integrated research program in Biscay (défi Gascogne). Particular thanks go to Pierre Beillois who developed efficient tools for data extraction from the output files of the hydrodynamic model.

References

Allain, G., Petitgas, P., and Lazure, P. 2001. The influence of mesoscale ocean processes on anchovy (Engraulis encrasicolus) recruitment in the Bay of Biscay estimated with a three-dimensional hydrodynamic model. Fisheries Oceanography, 10: 151-163.

Dazy, F. and Le Barzic, J.-F. 1996. L'analyse des données évolutives. Editions Technip, Paris, 227pp.

Lazure, P. and Jégou, A.-M. 1998. 3D modelling of seasonal evolution of Loire and Gironde plumes on Biscay bay continental shelf. Oceanologica Acta, 21: 165-177.

Lebart, L., Morineau, A., and Piron, M. 1995. Statistique exploratoire multidimensionnelle. Dunod, Paris, 439pp.

Petitgas, P. 2002. Distances et classifications de trajectoires. Note interne EcoHal, 3 janvier 2002. IFREMER/DRV/RH/EcoHal – Nantes, 14pp.

Table 1: Frequency of hodograph types in each year and for all years pooled.

	G1.hodo	G2.hodo	G3.hodo	G4.hodo	G5.hodo	G6.hodo
1985	0.011	0.720	0.000	0.247	0.011	0.011
1986	0.011	0.731	0.000	0.237	0.011	0.011
1987	0.065	0.570	0.043	0.301	0.011	0.011
1988	0.097	0.419	0.043	0.387	0.011	0.043
1989	0.172	0.398	0.043	0.366	0.011	0.011
1990	0.054	0.570	0.032	0.323	0.011	0.011
1991	0.054	0.570	0.032	0.323	0.011	0.011
1992	0.054	0.602	0.043	0.280	0.011	0.011
1993	0.161	0.419	0.032	0.387	0.000	0.000
1994	0.075	0.538	0.032	0.333	0.011	0.011
1995	0.172	0.484	0.032	0.290	0.011	0.011
1996	0.108	0.462	0.043	0.366	0.011	0.011
1997	0.097	0.430	0.043	0.409	0.011	0.011
1998	0.075	0.548	0.032	0.323	0.011	0.011
1999	0.054	0.548	0.043	0.290	0.011	0.054
2000	0.065	0.581	0.000	0.301	0.011	0.043
1985-2000	0.08	0.54	0.03	0.32	0.01	0.02

Table 2: average spatial frequency in each group of years for each hodograph type

	G1.hodo	G2.hodo	G3.hodo	G4.hodo	G5.hodo	G6.hodo
G1.year	0.134	0.435	0.039	0.367	0.009	0.014
G2.year	0.062	0.566	0.032	0.309	0.011	0.020
G3.year	0.011	0.726	0.000	0.242	0.011	0.011

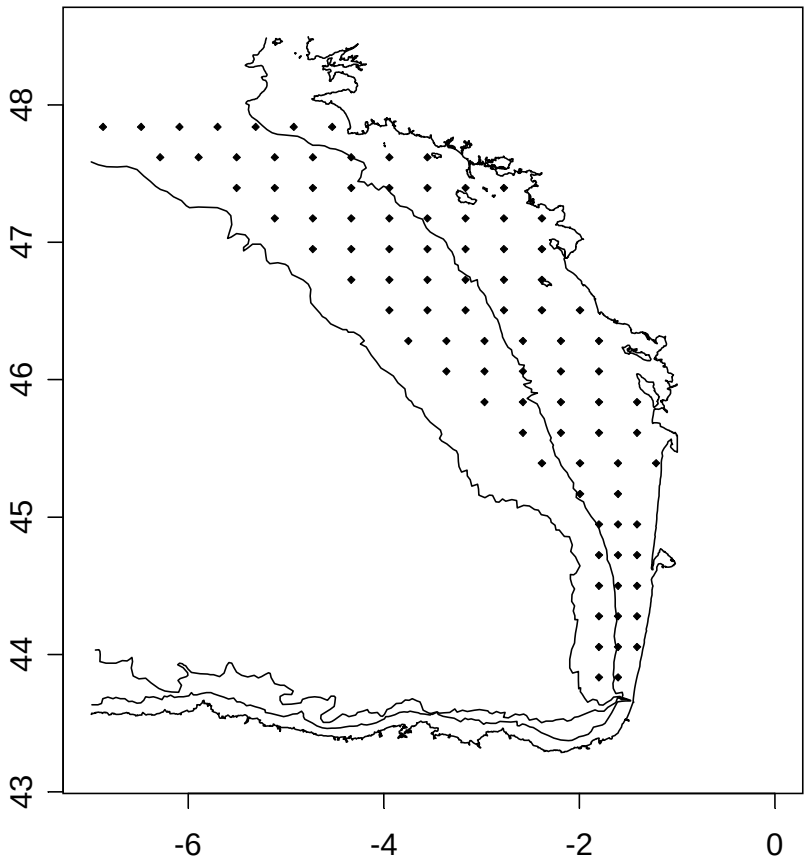

Fig. 1: Grid of 93 station points (black diamonds) at which the annual hodographs were estimated. Lines shown are the coast and the isobaths 100 m and 200 m.

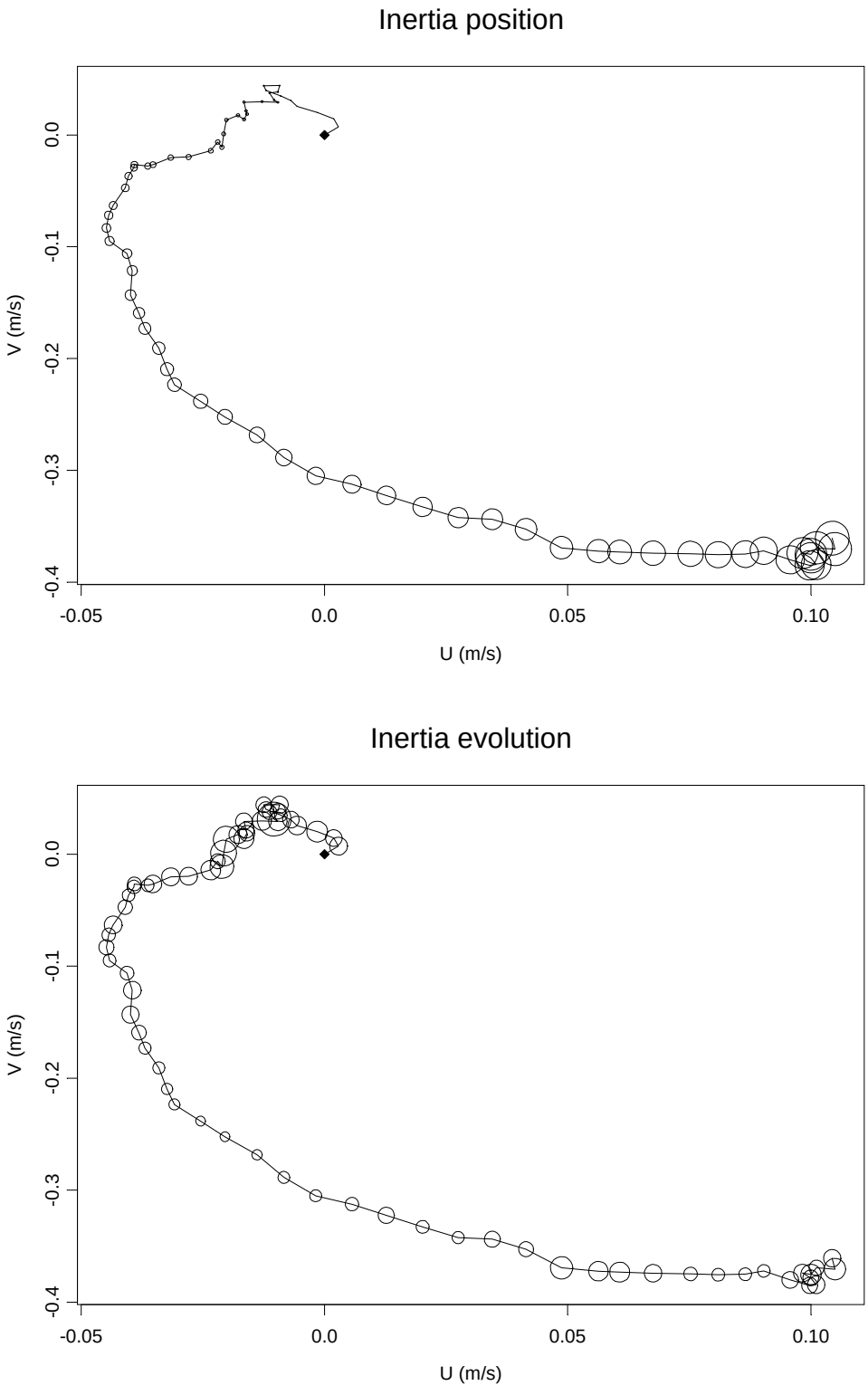

Fig. 2: Inertia position and evolution superimposed on the average hodograph (all years and points pooled). The black diamond represents the hodograph start.

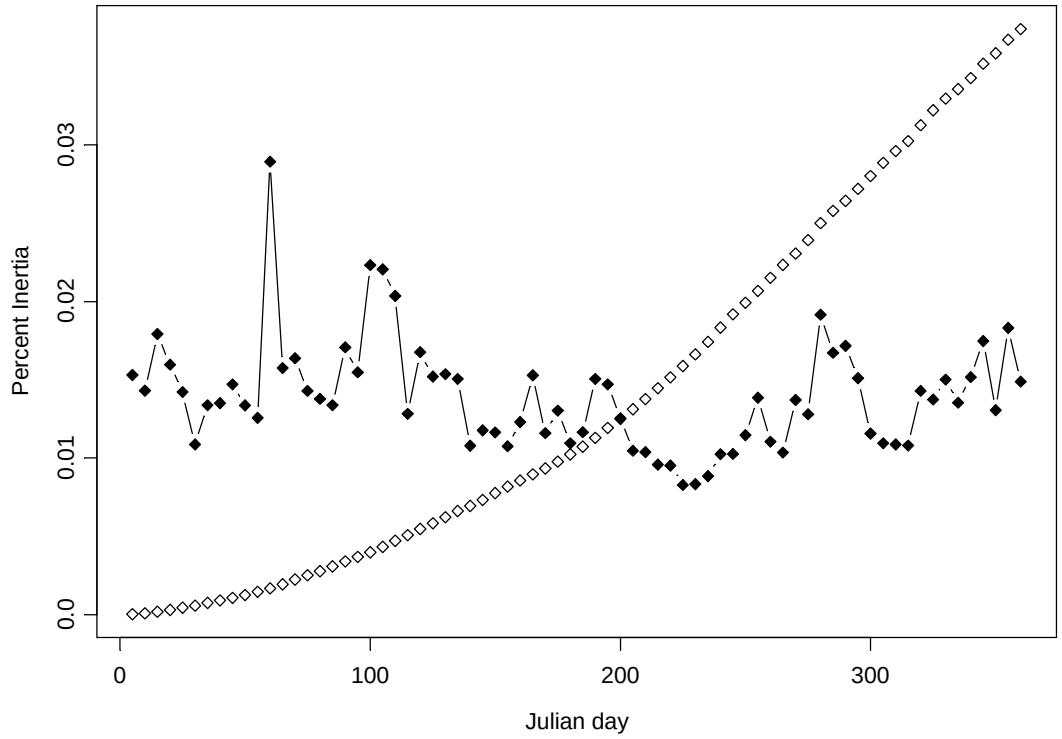

Fig. 3: Percent of inertia evolution (black diamonds) and position (white circles) along the average hodograph (all years and points pooled).

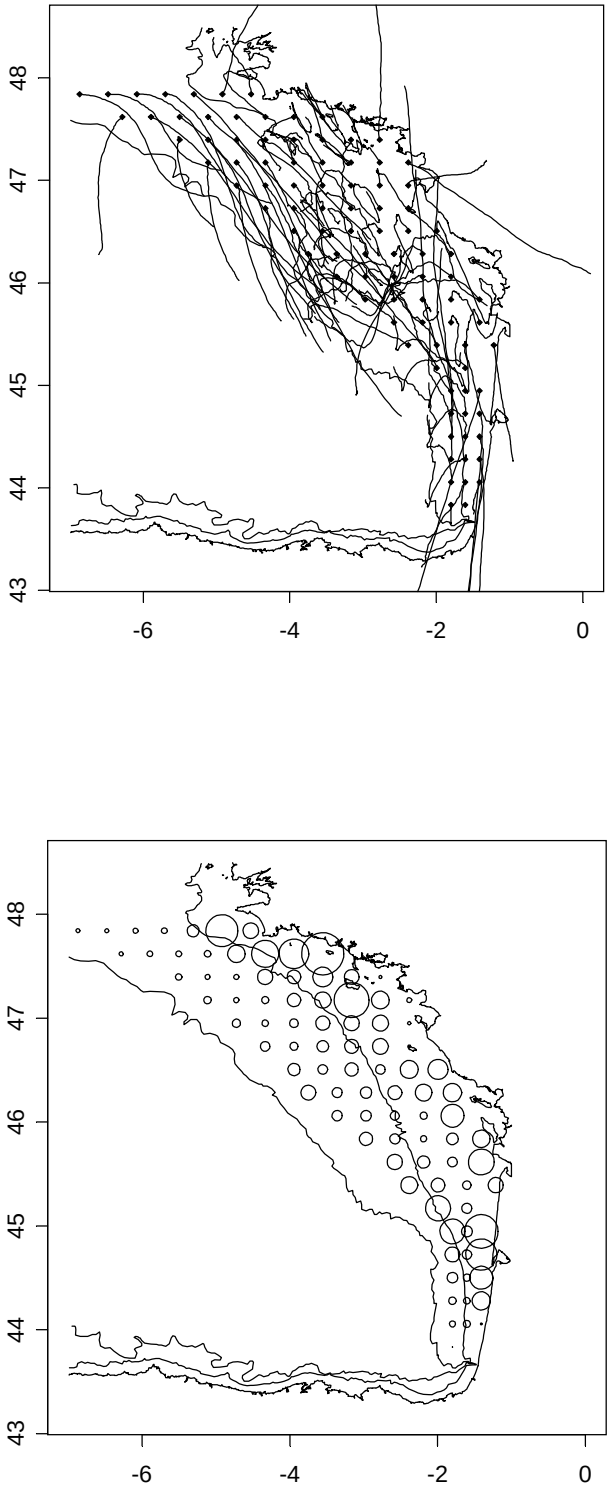

Fig. 4: Above: Annual hodogaphs of surface currents (10 m) at each point averaged over the years (1985-2000). Below: Inertia corresponding to the distance compromise at each point over the years.

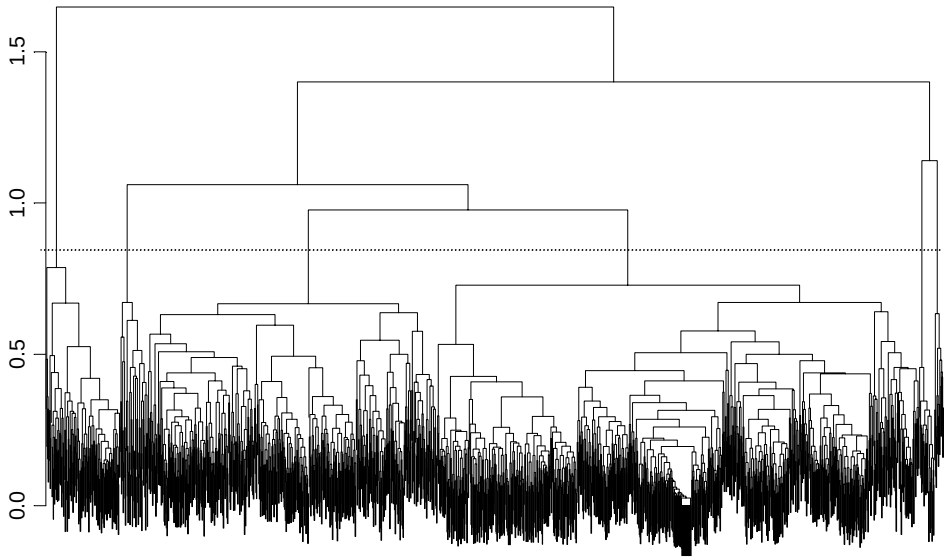

Fig. 5: Hierarchical classification of the 1488 hodographs based on the compromise distance between them. The dashed line represents the 6 groups retained for the typology.

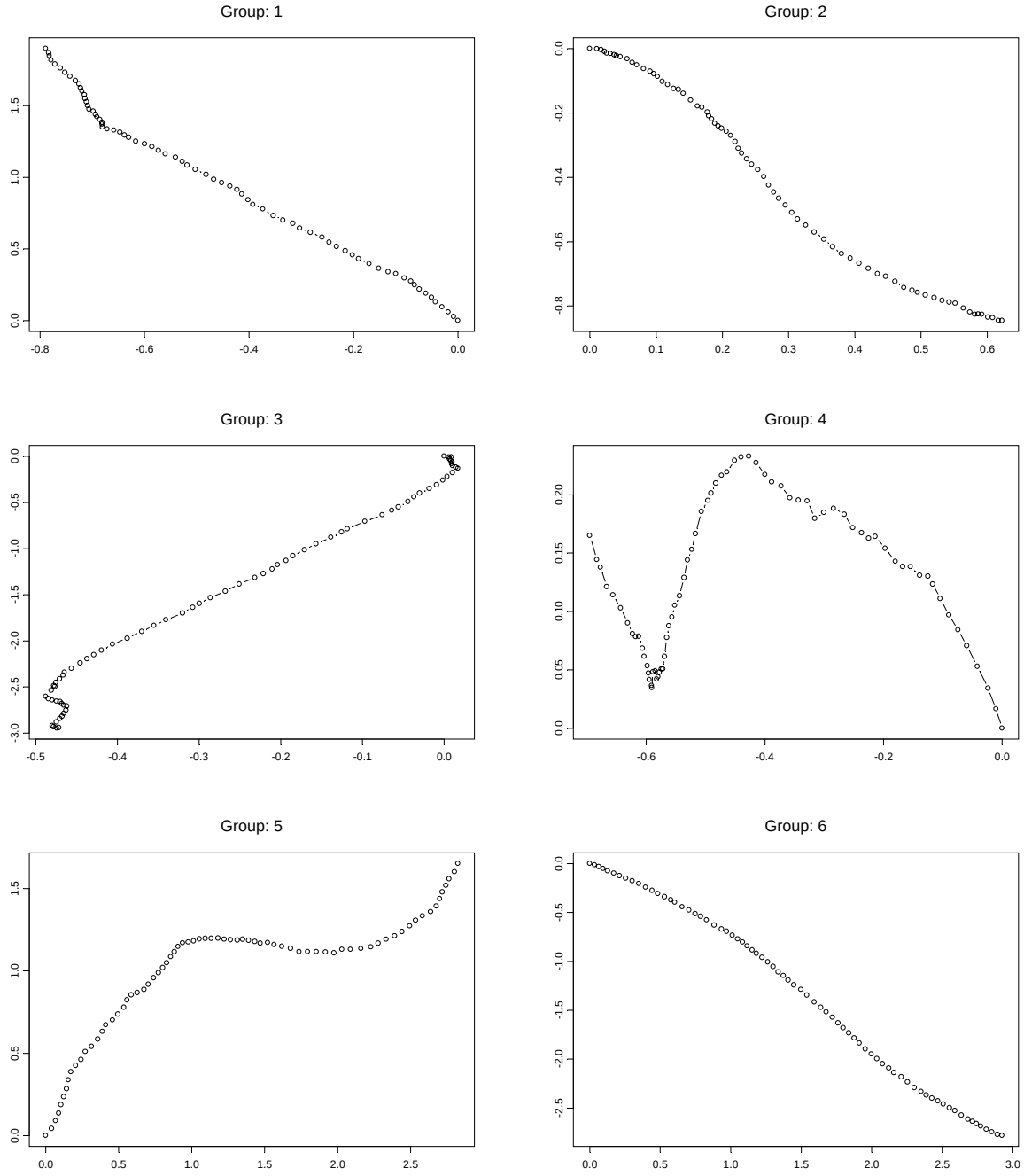

Fig. 6: Typology of hodographs. Average hodograph per group obtained cutting the hiearchical classification tree.

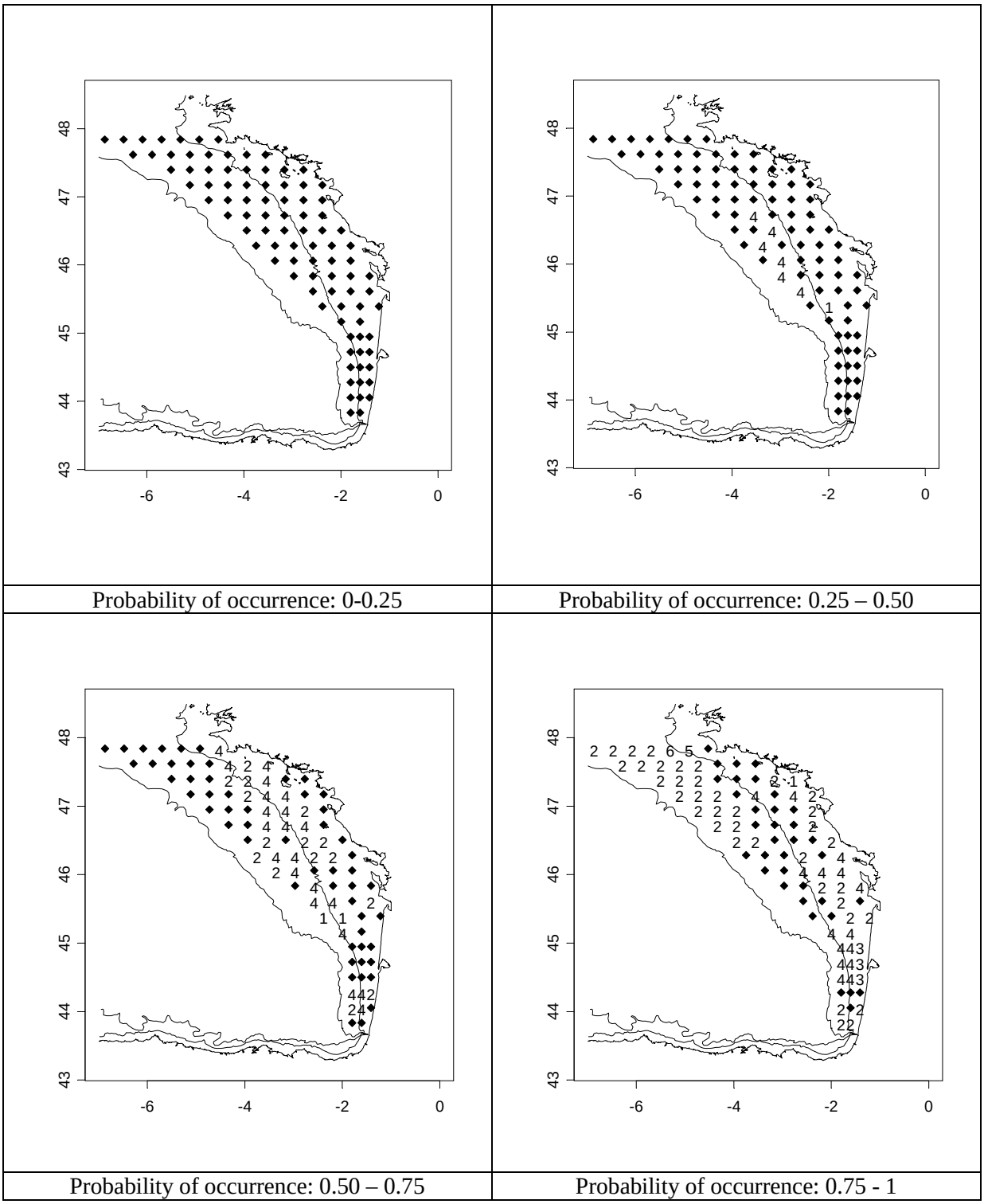

Fig. 7: Maps hodograph types with varying inter-annual probability of occurrence at each point.

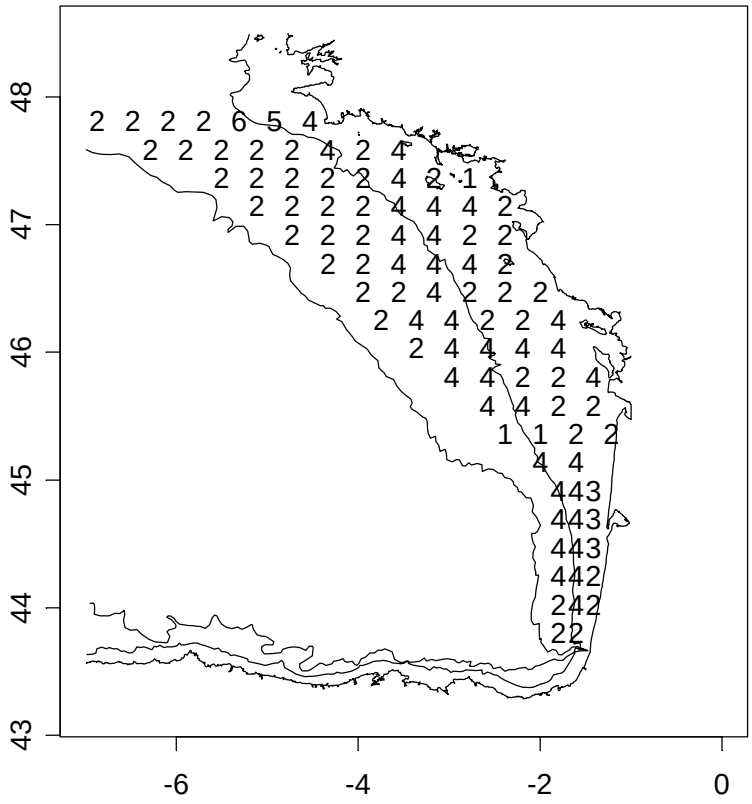

Fig. 8: Synthetic map of hodograph types with highest inter-annual probability at each point. All probabilities greater than 0.4.

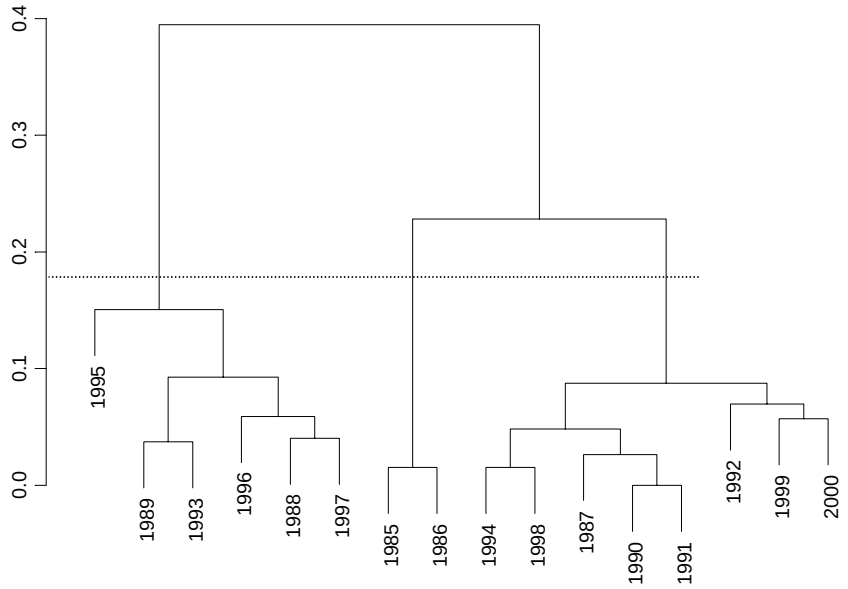

Fig. 9: hierarchical classification tree of the years (compact method) based on the Euclidean distance between yearly spatial frequencies of hodograph types. The dashed line represents the 3 groups of years retained.